Tectonic Tremors in the Northern Mexican Subduction Zone Remotely Triggered by the 2017 Mw8.2 Tehuantepec Earthquake

Masatoshi Miyazawa (miyazawa@rcep.dpri.kyoto-u.ac.jp)
Kyoto University https://orcid.org/0000-0002-3319-1216
Miguel Ángel Santoyo
Universidad Nacional Autonoma de Mexico Direccion General de Bibliotecas: Universidad Nacional Autonoma de Mexico

Full paper

Keywords: 2017 Tehuantepec earthquake, tectonic tremor, remote triggering, wavefield simulation

Posted Date: September 8th, 2020

DOI: https://doi.org/10.21203/rs.3.rs-73471/v1

Version of Record: A version of this preprint was published on January 4th, 2021. See the published version at https://doi.org/10.1186/s40623-020-01331-x.

Abstract

Surface waves from the 2017 Mw8.2 Tehuantepec earthquake remotely triggered tectonic tremors in the Jalisco region, approximately 1000 km WNW in the northern Mexican subduction zone. This is the first observation of tremor triggering in this region and one of the largest known examples of triggered tremor in the world. While prior studies found tectonic tremors triggered by teleseismic waves in subduction zones and plate boundaries, further investigation of tremor triggering is crucially important for understanding the causative mechanism. We calculate the stress and strain changes across the three-dimensional plate interface attributable to seismic waves from the earthquake by full wavefield simulation. The maximum magnitude of the dynamic strain tensor eigenvalues on the plate interface, where tremors likely occur, is approximately 10^{-6}. The subducting slab geometry effectively amplifies triggering waves. The triggering Coulomb failure stress changes resolved for a thrust fault plane consistent with the geometry are estimated at approximately 10-40 kPa. The relationship between the triggering stress and triggered tremor amplitude may indicate that the $a\sigma$ of the rate-state-dependent friction law is 10 to 100 kPa.

Introduction

Large earthquakes can remotely trigger tectonic tremors as well as earthquakes at great distances during the passage of seismic waves through regions close to failure. Previous studies found that tectonic tremors immediately triggered by teleseismic waves in subduction zones and at plate boundaries around the world, including the Nankai subduction zone (e.g., Miyazawa and Mori 2005, 2006), the Cascadia subduction zone (e.g., Rubinstein et al. 2007), Taiwan (e.g., Peng and Chao 2008), the Hikurangi subduction zone (Fry et al. 2011), the Mexican subduction zone (Zigone et al. 2012), and the San Andreas Fault (e.g., Ghosh et al. 2009; Hill et al. 2013), where ambient tremors have also been reported. The amplitudes of triggered tremors are highly correlated with the peaks of passing waves. These findings are not only intriguing because transient stress changes can stimulate a fault to slip but also remarkably important for understanding the mechanism that causes tectonic tremors, which are still enigmatic phenomena at plate interfaces. For example, Rubinstein et al. (2007) and Miyazawa and Brodsky (2008) showed that movements enhancing the plate movement played an important role in triggering tremors, indicating the mechanism of slip on the plate interface.

We show that tectonic tremors in the northern Mexican subduction zone, i.e., Rivera and Cocos subduction zones beneath the Jalisco region, where tremor triggering has not been reported previously, were remotely triggered by the 2017 Mw8.2 Tehuantepec earthquake approximately 1000 km to the southeast. The 2017 Tehuantepec earthquake occurred at 04:49:46.7 on September 8, 2017 (UTC) (global centroid moment tensor (CMT) catalog), in the southern Mexican subduction zone with a mechanism of normal faulting within the Cocos Plate and ruptured the whole thickness of the Cocos Plate down to the mantle (e.g., Melgar et al. 2018; Suárez et al. 2019). Notably, the 2017 Tehuantepec earthquake is also known to have triggered tremors along the western coast of North America (Chao et al. 2017) and activated tremors in the southern Mexican subduction zone (Husker et al. 2019). In the southern Mexican

subduction zone, tremors were triggered by the 2010 Mw8.1 Maule earthquake accompanied by slow slip (Zigone et al. 2012). Since triggered tremors previously found around the world are located in different tectonic settings, a comparison of the triggering process is required to help us comprehensively clarify the source mechanism. This study investigates the characteristic triggering process by calculating strain and stress changes at depth using a forward technique of elastic wave simulation for a three-dimensional structure and by estimating the friction parameter from the observed waves.

Detection Of Triggered Tremors

The triggered tremors with dominant periods ≤ 1 s during the passage of surface waves with dominant periods of approximately 20 s can be detectable by simple signal processing with high-pass filtering. Figure 1 shows the velocity waveforms for the Mw8.2 Tehuantepec earthquake at station CJIG of the National Seismological Service (SSN) of Mexico (SSN 2017) (Fig. 2). The high-pass filtered waveforms at 8 Hz in Fig. 1a show the tremor recurrently and periodically triggered during the passage of surface waves (Fig. 1b). Three tremors were triggered in phase with passing surface waves from 310 s to 380 s after the earthquake initiation, while they seemed to be followed by further tremor activity with smaller amplitudes, including two minor tremors. These characteristics are very similar to the dynamically triggered tectonic tremors previously found. Comparing the high- and low-frequency components, we can identify that the first-arrival high-frequency waves from 140 s to 240 s represent the P-wave arrival and its coda waves, and the second ones from 250 s to 300 s correspond to the arrival of the S-wave. These high-frequency signals at the arrivals of P- and S-waves were also observed at other stations. Both P- and S-waves are known to be capable of triggering tectonic tremors (Miyazawa 2012; Hill et al. 2013); however, we could not distinguish tremors from teleseismic body waves in the present study. The amplitude of large triggered tremors here observed exceeds 1 μm/s, which is roughly one order of magnitude larger than that of the background tremors.

We could not identify any transiently triggered tremors at other tremor regions in the Mexican subduction zone, e.g., Oaxaca and Guerrero, close to the 2017 Tehuantepec earthquake, where Zigone et al. (2012) found triggered tremor, using both broadband and strong-motion records, because the codas of body waves arrive together with the surface waves and hinder the detection of tremors by high-pass filtering. Other techniques, such as the reference spectrum method (Miyazawa 2012), might be useful for detection; however, in this case, a dense seismic network for a statistical test and a reference event are required. This situation does not mean that no transiently triggered tremors occurred in other areas because Husker et al. (2019) found clear signs of tremor burst, particularly in Oaxaca subsequent to the 2017 Tehuantepec earthquake, and the activity might have started during the passage of the seismic waves.

The locations of the triggered tremors were not obtained because of the relatively low spatial coverage of the seismic network. The two closest stations to CJIG are located within approximately 180 km to 220 km, which are too far to observe these triggered tremors. Further, because CJIG is the only station that recorded the triggered tremors, they likely occurred in the region of background tremor activity, similar

to the results of previous studies (Brudzinski et al. 2016; Maury et al. 2018). The magnitudes are also not available, although the tremors that exceed 1.5 μm/s in amplitude could be the largest triggered tremors ever recorded in the world.

Full Wavefield Simulation For The 2017 Tehuantepec Earthquake

We examine the strain and stress changes on the plate interface, where tremors likely occur, associated with passing seismic waves from the 2017 Tehuantepec earthquake. For this purpose, the inverse approach using observed waveforms at a single station near the source via transport kernels in a one-dimensional structure (Miyazawa and Brodsky 2008; Miyazawa 2019) is applicable. However, the exact location of the triggered tremors is unknown, and the triggering wave propagates along the trench and is significantly affected by the structure of the subducting slab. Therefore, we first obtain an overview of the spatial distribution of these changes from the full waveform simulation in the three-dimensional structure. We use an open-source seismic wave propagation code (OpenSWPC) by Maeda et al. (2017) for elastic wave simulation. This approach solves the equations of motion in three-dimensional Cartesian coordinates with viscoelastic constitutive equations using a finite difference method. The spatial grid size is 1 km in the horizontal and vertical directions, and the time step is 0.05 s. The computational region has an area of 1000 km × 2000 km and extends from the topographic surface to a depth of 1000 km (Fig. 2). The distance is measured based on the Gauss-Krüger coordinate system, where the source location of the Tehuantepec earthquake is set as the origin. The structure model is made by combining ETOPO1 for topography (Amante and Eakins 2009), CRUST 1.0 (Laske et al. 2013) for the crust including the Moho, and Slab2 (Hayes et al. 2018) for the subducting plate. The subduction zone geometry model of Slab2 for Central America is extrapolated to cover a wider area for the numerical simulation using the surface command in the Generic Mapping Tool (GMT) (Wessel and Smith 1998) with a tension factor of 0.25. Seawater fills from the ocean floor to the surface. We do not employ spherical structures. Table 1 shows the parameters used for the structure, where we refer to and modify the values of the Japan integrated velocity structure model (Koketsu et al. 2012). We assume a point source obtained by the W-phase inversion (Ye et al. 2017) with a moment rate function of the Herrmann function. Table 2 shows the source parameters of the Tehuantepec earthquake, where the rise time is determined through trial and error.

Table 1
Structure model used for the full wavefield simulation.

Layer	Density (g/cm^3)	Vp (km/s)	Vs (km/s)	Qp	Qs
Topography (ETOPO1)	2.11	2.70	1.20	200	100
Crust 1	2.67	6.20	3.70	680	400
Crust 2	2.69	6.60	3.90	680	400
Crust 3 (Moho)	3.20	7.50	4.40	850	500
Slab Top (Slab2)	2.65	5.90	3.50	425	250
Slab (Oceanic Moho)	3.20	8.00	4.60	850	500

Table 2
Source parameters of the 2017 Tehuantepec earthquake.

Longitude	Latitude	Depth	Mw	Strike	Dip	Rake	Rise time
265.69°	15.34°	50 km	8.21	313°	77.7°	-95.5°	32 s

Figure 1b shows the recorded and simulated waveforms at CJIG, which were bandpass filtered at 0.01 to 0.10 Hz. Note that the times of the simulated waves were shifted by -16 s considering the duration time. The reconstruction of the full wavefield is particularly difficult in a subduction zone (e.g., Takemura et al. 2019), but the simulated waveforms, nevertheless, are generally consistent with recorded data for all the components except for the amplitudes of higher frequency surface waves after 350 s. Similar trends can be seen at the other stations along the trench. Considering the radiation pattern of surface waves, as the station is located near the extension of a nodal plane, the vertical and radial components are highly sensitive to the strike direction. Since the simulated P-waves are consistent with the recorded ones and the simulated Love waves cannot reconstruct the high amplitudes after 350 s, the differences are likely caused by the uncertainties in the three-dimensional structures, including heterogeneities, and by the assumption of a point source model to a certain extent. We examine the wavefield simulation using finite fault models with slip distributions, while there is no improvement of simulated waveforms at CJIG to fit the observed ones for this frequency range. The tomography studies on phase and group velocity inversion using surface wave observed in Mexico show strong horizontal heterogeneities in the crust between the 2017 event location and CJIG (e.g., Gaite et al. 2012; Castellanos et al. 2018), which are sensitive to the 10 s to 20 s surface wave features. Furthermore, the spherical structure is not modeled in the simulation, although this factor may have less influence than the reasons mentioned above. The present results are sufficiently robust to investigate the characteristics of the wavefields since our purpose is not to examine the exact structure or source model.

An additional movie file shows the simulated wavefields at a depth of 7 km [Additional file 1]. The seismic waves seem to propagate slightly slower onshore than offshore due to the slow velocity structure in the upper mantle. The waves propagating along the onshore toward the northwest direction, where the

triggered tremors were observed, are accompanied by longer codas, which are caused by the wedge mantle structure between the crust and the subducted slab. This structure can also increase the amplitudes of surface waves, while the observed large amplitudes in the coda are not fully simulated.

Strain And Stress Estimation

Based on the full waveform simulation, we obtain the maximum magnitudes of eigenvalues of the dynamic strain tensor given as the representative maximum strain load at each position. Figure 3a shows the spatial distribution of maximum strain changes on the plate interface of Slab2. The value of strain changes generally decreases with distance from the epicenter. Anomalies of substantial strain changes are observed in the Guerrero and Jalisco regions to the northwest along the trench, where the plate interfaces are shallower than those in other regions. In the Jalisco region, the stress/strain changes have larger values within the tremor region than in the shallower or deeper regions (Fig. 3b). The maximum strain changes in the Jalisco tremor region are estimated at approximately 1×10^{-6}, which is one to two orders of magnitude larger than the changes due to the earth tide. Note that these values may underestimate the actual ones because the simulated maximum amplitudes of surface waves underestimate the actual maximum amplitudes.

We then estimate the stress changes resolved for the mechanism of the tectonic tremor. We assume that the tremor occurs on the plate interface with a mechanism having a strike of 319°, a dip of 29° and a rake of 90° for a fault plane consistent with the subducting slab geometry. Since the exact location of the triggered tremor is not available, we substitute the median epicenter of ambient tremors using the tremor catalog in Jalisco by Idehara et al. (2014), which is located approximately 50 km to the east of station CJIG. We estimate the change in the Coulomb failure stress at the hypocenter on the plate interface, $\Delta\tau + \mu'\Delta\sigma_n$, where the effective friction coefficient μ' is assumed to be 0.2 and $\Delta\tau$ and $\Delta\sigma_n$ are the shear stress change in the slip direction and the normal stress change on the fault plane (negative for compression), respectively (Fig. 4). The waveforms are bandpass filtered at 0.01 to 0.10 Hz. The Lamé parameters are set by the structure model in Table 1 for the synthetic case (Fig. 4a). We also use a linear kernel approach that computes continuous waveforms spanning the full spectrum at depth (Miyazawa and Brodsky 2008; Miyazawa 2019) to calculate the dynamic stress change resolved for the tremor mechanism at the depth of the plate interface. In this method, the stress changes associated with passing surface waves can be obtained from surface observations. For simplicity, we assume fundamental mode Rayleigh and Love waves propagating in an isotropic elastic medium. The Lamé parameters λ and μ are both 66 GPa at this depth, and the other parameters are the same as those described in Miyazawa (2019). Figure 5b shows the stress changes beneath station CJIG at a depth of 45 km. A systematic time difference in the arrival times of stress peaks between the simulation and estimation based on the observations occurs because of the difference in the location where we obtained the stress changes. As we cannot locate the triggered tremor source, we do not correct for traveltime from the tremor source to station CJIG to directly compare the stress changes and corresponding tremor amplitudes. However, the triggering stresses for the three tremors in Fig. 1 may correspond to the three peaks of 34.6 kPa, 38.2 kPa, and 9.1 kPa at times from

300 s to 370 s for the simulation (Fig. 4a) and of 14.7 kPa, 28.4 kPa, and 22.6 kPa from 310 s to 380 s for the estimation from the observations (Fig. 4b). The differences in these values appear primarily because the parameters and structures assumed in the simulation and estimation models are different and probably because station CJIG is located closer to the trench where the amplitudes of seismic waves become smaller than those in the tremor region.

Large stress changes could likely trigger tremors; however, the observation of three tremors may not be enough to clarify the relationship between the amplitudes of triggered tremors and triggering stress, as shown by Miyazawa and Brodsky (2008). Since the tremor hypocenters are not obtained, we simply compare the peak values of tremor amplitude in the vertical component and the triggering stress (Fig. 5), where the peak tremor amplitudes are measured from the envelope of high-pass filtered waveforms (Fig. 1a) with 1 Hz lowpass filtering and the stress changes are estimated by the waveforms recorded at CJIG (Fig. 4b). Two more small triggered tremors following three large ones are also used. Simulated values are not used here because the largest surface waves are not reconstructed. If we assume that the triggered tremors occurred at the same place, the relationship between the triggered tremor amplitude and the triggering stress derived by Miyazawa and Brodsky (2008) can be applicable to the peak values. The peak tremor amplitude, Tamp, is represented by

$$\mathrm{T}_{amp} = Ca\sigma\left[\exp\left(\frac{\Delta CFF}{a\sigma}\right) - 1\right],$$

where a is an empirically derived constant, σ is the background stress (Dieterich 1994) and C is a constant. The parameters are obtained as $a\sigma$ = 56.84 kPa and C = 0.01965, which may not be robust due to the small number of datasets. The model curve and those when $a\sigma$ is 1, 10 and 100 kPa are shown in Fig. 5, while there is no significant difference for $a\sigma$ > 100 kPa in this stress range. The relationship in our study may follow this model when $a\sigma$ ranges from 10 kPa to 100 kPa (Fig. 5), which is consistent with the case of tremor triggering found in the Nankai region (Miyazawa and Brodsky 2008).

Other Teleseismic Events

We investigate the dynamic triggering of tremors by teleseismic waves from other large earthquakes from 2011 to 2019. From the ANSS earthquake catalog, we selected M ≥ 7.0 teleseisms, of which the peak ground velocities (PGVs) are expected to exceed 1.0 mm/s for surface waves of 20 s at CJIG. The PGV is estimated by using an amplitude-magnitude relationship (e.g., van der Elst and Brodsky 2010; Chao et al. 2013). Table 3 shows that the selected six large earthquakes and the PGV values are the measured maximum amplitudes of the vector velocity from the three components bandpass filtered from 0.01 Hz to 0.10 Hz recorded at CJIG. We cannot find any evidence of triggered tremors due to these earthquakes, by using the same signal processing as mentioned above for the 2017 Tehuantepec earthquake. The observation that the triggered tremor only occurred for the 2017 Tehuantepec earthquake may be due to the large amplitude of the triggering waves. However, the amplitude of waves that triggered the first tremor in 2017 (Fig. 1) is comparative to PGVs of the 2012 Mw7.4 and 2014 Mw7.2 earthquakes. There

may be no clear threshold to trigger tremors if the amplitude of potential triggering waves at the surface is less than 10 mm/s.

Table 3
PGV of other teleseismic earthquakes recorded at CJIG from 2011 to 2019.

Origin time (UTC)	Mw	Depth [km]	Distance [km]	PGV (mm/s)
2011-03-11	9.1	29	10,523	0.6147
2012-03-20	7.4	20	794	6.4976
2012-11-07	7.4	24	1,528	0.7079
2014-04-18	7.2	24	489	4.1535
2017-09-19	7.1	48	698	0.6566
2018-02-16	7.2	22	824	1.0696

Discussion

The main reasons why the tectonic tremors were triggered by the surface waves from the 2017 Tehuantepec earthquake include the large stress/strain changes in the tremor region. As shown in Fig. 3, substantial strain changes of about 1×10^{-6} along the background tremor region in Jalisco indicate that the surface waves can effectively trigger tremors. The Coulomb failure stress changes effective for the triggering range from 10 to 40 kPa. These large stress/strain changes are one to two orders of magnitude larger than those from earth tides and present abnormally large values. Note that these high values are also produced by the geometry of the subduction zone and the spatial relationship between the tremor region and the triggering earthquake, as seen in the full wavefield simulation. The results may indicate that the stress changes associated with passing P- and S-waves, which are comparable to the lowest triggering stress from the surface waves, were also capable of triggering the tremor. To date, we have not found clear evidence of triggering from body waves generated by the 2017 Tehuantepec earthquake.

The amplitude of triggered tremors of 1 μm/s is very large, roughly one order of magnitude larger than the amplitude of background ambient tremors, and one of the largest triggered tremor ever reported. The triggered tremors during the passage of surface waves are well known to sometimes have significant amplitude corresponding to large triggering stress because of a large slip area or alternatively because of the simultaneous occurrence of numerous events (Miyazawa and Brodsky 2008) and/or the triggering associated with slow slip (Miyazawa 2012). In the present case, no observation of slow slip events or activation of tremors in Jalisco subsequent to the 2017 Tehuantepec earthquake has been reported (Husker et al. 2019; personal communication) because the tremor catalog cannot be verified at only the single station CJIG. The transient stress changes either by body waves or surface waves indeed induced slip on the fault, thereby causing tremors, but the tremor activity might not have been followed by aftershock-like activity and might have returned to a low background level because the fault was not

initially close to failure. This interpretation is similar to the characteristics of triggered seismicity with relatively large magnitude, as seen for the case of a dynamically triggered moderate earthquake, where the aftershocks abruptly returned to background levels within a month (Miyazawa 2016). If there was either triggered or background slow slip in Jalisco only when the 2017 Tehuantepec earthquake occurred, although such event has not been detected yet, this is consistent with no observation of triggered tremor by the similar amplitude of triggering waves from other large earthquakes. The tremor activity in Oaxaca subsequent to the 2017 Tehuantepec earthquake may have been caused by both dynamic and static stress changes (Husker et al. 2019).

Conclusions

The discovery of triggered tremors from the 2017 Mw8.2 Tehuantepec earthquake in the Jalisco region, as well as in the Oaxaca region as previously reported, indicates the possibility of the dynamic triggering of tremors in any other tremor region. Moreover, the relationship between the triggering stress and the triggered tremor amplitude seems to be similar to previous findings. This result suggests that more investigation of triggered tremors through continuous observations can systematically provide us with important information about friction parameters on the plate interface, which might be useful for earthquake cycle simulation in the subduction zone.

List Of Abbreviations

CMT: centroid moment tensor

GMT: Generic Mapping Tools

PGV: peak ground velocity

Declarations

Ethics approval and consent to participate

Not applicable

Consent for publication

Not applicable

Availability of data and materials

The SSN data were obtained by the Servicio Sismológico Nacional (México), and station maintenance, data acquisition and distribution are thanks to its personnel. The figures were generated using GMT (Wessel and Smith 1998).

Competing interests

The authors declare that they have no competing interests.

Funding

This work was supported by the Japan Science and Technology Agency (JST) and the Japan International Cooperation Agency (JICA) under its Science and Technology Research Partnership for Sustainable Development (SATREPS) project (JPMJSA1510) (MM and MS) and partially supported by JSPS KAKENHI Grant Number JP16K05537 and JSPS Grant Number JPMXS05G2900001 (MM). This work was partially supported by CONACYT PN-2015-639 project (MS).

Authors' contributions

MM contributed to the simulation and modeling, and MS involved in signal processing. Both authors discussed the results and commended on the manuscript.

Acknowledgements

Discussion with Allen Husker and Naofumi Aso helped develop this study. For data analysis, we used the computer systems of the Earthquake and Volcano Information Center of the Earthquake Research Institute (ERI), University of Tokyo, Japan.

References

1. Amante C, Eakins BW (2009) ETOPO1 Global Relief Model converted to PanMap layer format. NOAA-National Geophysical Data Center, PANGAEA. doi:10.1594/PANGAEA.769615.
2. Bird P (2003) An updated digital model of plate boundaries. Geochem Geophys Geosystems 4:1027. doi:10.1029/2001gc000252.
3. Brudzinski M, Schlanser K, Kelly N, Demets C, Grand S, Azúa B, Cabral-Cano E (2016) Tectonic tremor and slow slip along the northwestern section of the Mexico subduction zone. Earth Planet Sci Lett 454:259-271. doi:10.1016/j.epsl.2016.08.004.
4. Castellanos JC, Clayton RW, Pérez-Campos X (2018) Imaging the eastern trans-Mexican volcanic belt with ambient seismic noise: evidence for a slab tear. J Geophys Res: Solid Earth 123:7741-7759. doi:10.1029/2018JB015783.
5. Chao K, Gonzalez-Huizar H, Tang V, Klaeser RD, Mattia M, Van der Lee S (2017) Global examination of triggered tectonic tremor following the 2017 Mw8.1 tehuantepec earthquake in Mexico. AGU fall meeting, S33G-2369, New Orleans, 11-15 December 2017.
6. Chao K, Peng Z, Gonzalez-Huizar H, Aiken C, Enescu B, Kao H, Velasco AA, Obara K, Matsuzawa T (2013) A global search for triggered tremor following the 2011 Mw 9.0 Tohoku earthquake. Bull Seismol Soc Am 103:1551-1571. doi:10.1785/0120120171.

7. Dieterich J (1994) A constitutive law for rate of earthquake production and its application to earthquake clustering. J Geophys Res: Solid Earth 99:2601-2618. doi:10.1029/93jb02581.
8. Fry B, Chao K, Bannister S, Peng Z, Wallace L (2011) Deep tremor in New Zealand triggered by the 2010 Mw8.8 Chile earthquake. Geophys Res Lett 38:L15306. doi:10.1029/2011gl048319.
9. Gaite B, Iglesias A, Villaseñor A, Herraiz M, Pacheco JF (2012) Crustal structure of Mexico and surrounding regions from seismic ambient noise tomography. Geophys J Int 188:1413-1424. doi:10.1111/j.1365-246X.2011.05339.x.
10. Ghosh A, Vidale JE, Peng Z, Creager KC, Houston H (2009) Complex nonvolcanic tremor near Parkfield, California, triggered by the great 2004 Sumatra earthquake. J Geophys Res: Solid Earth 114:B00A15. doi:10.1029/2008jb006062.
11. Hayes GP, Moore GL, Portner DE, Hearne M, Flamme H, Furtney M, Smoczyk GM (2018) Slab2, a comprehensive subduction zone geometry model. Science 362:58-61. doi:10.1126/science.aat4723.
12. Hill D, Peng Z, Shelly D, Aiken C (2013) S-wave triggering of tremor beneath the Parkfield, California, section of the San Andreas fault by the 2011 Tohoku, Japan, Earthquake: observations and theory. Bull Seismol Soc Am 103:1541-1550. doi:10.1785/0120120114.
13. Husker A, Frank WB, Gonzalez G, Avila L, Kostoglodov V, Kazachkina E (2019) Characteristic tectonic tremor activity observed over multiple slow slip cycles in the Mexican subduction zone. J Geophys Res: Solid Earth 124:599-608. doi:10.1029/2018jb016517.
14. Idehara K, Yabe S, Ide S (2014) Regional and global variations in the temporal clustering of tectonic tremor activity. Earth Planets Space 66:66. doi:10.1186/1880-5981-66-66.
15. Koketsu K, Miyake H, Suzuki H (2012) Japan integrated velocity structure model version 1. In: Proceedings of the 15th world conference on earthquake engineering. Lisbon, Portugal, p 1773.
16. Laske G, Masters G, Ma Z, Pasyanos M (2013) Update on CRUST1.0 - A 1-degree global model of Earth's crust. EGU General Assembly, EGU2013-2658, Vienna 7-12 April 2013
17. Maeda T, Takemura S, Furumura T (2017) OpenSWPC: an open-source integrated parallel simulation code for modeling seismic wave propagation in 3D heterogeneous viscoelastic media. Earth Planets Space 69:102. doi:10.1186/s40623-017-0687-2.
18. Maury J, Ide S, Cruz-Atienza VM, Kostoglodov V (2018) Spatiotemporal variations in slow earthquakes along the Mexican subduction zone. J Geophys Res: Solid Earth 123:1559-1575. doi:10.1002/2017jb014690.
19. Melgar D, Ruiz-Angulo A, Garcia ES, Manea M, Manea VC, Xu X, Ramirez-Herrera MT, Zavala-Hidalgo J, Geng J, Corona N, Pérez-Campos X, Cabral-Cano E, Ramirez-Guzmán L (2018) Deep embrittlement and complete rupture of the lithosphere during the Mw 8.2 tehuantepec earthquake. Nat Geosci 11:955-960. doi:10.1038/s41561-018-0229-y.
20. Miyazawa M (2012) Detection of seismic events triggered by P-waves from the 2011 Tohoku-Oki earthquake. Earth Planets Space 64:1223-1229. doi:10.5047/eps.2012.07.003.
21. Miyazawa M (2016) An investigation into the remote triggering of the Oita earthquake by the 2016 Mw 7.0 Kumamoto earthquake using full wavefield simulation. Earth Planets Space 68:205.

doi:10.1186/s40623-016-0585-z.

22. Miyazawa M (2019) Bayesian approach for detecting dynamically triggered very low-frequency earthquakes in the Nankai subduction zone and application to the 2016 Mw 5.9 off-Kii Peninsula earthquake, Japan. Geophys J Int 217:1123-1140. doi:10.1093/gji/ggz073.
23. Miyazawa M, Brodsky EE (2008) Deep low-frequency tremor that correlates with passing surface waves. J Geophys Res: Solid Earth 113:B01307. doi:10.1029/2006jb004890.
24. Miyazawa M, Mori J (2005) Detection of triggered deep low-frequency events from the 2003 Tokachi-oki earthquake. Geophys Res Lett 32:L10307. doi:10.1029/2005gl022539.
25. Miyazawa M, Mori J (2006) Evidence suggesting fluid flow beneath Japan due to periodic seismic triggering from the 2004 Sumatra-Andaman earthquake. Geophys Res Lett 33:L05303. doi:10.1029/2005gl025087.
26. Peng Z, Chao K (2008) Non-volcanic tremor beneath the central range in Taiwan triggered by the 2001 Mw 7.8 Kunlun earthquake. Geophys J Int 175:825-829. doi:10.1111/j.1365-246X.2008.03886.x.
27. Rubinstein JL, Vidale JE, Gomberg J, Bodin P, Creager KC, Malone SD (2007) Non-volcanic tremor driven by large transient shear stresses. Nature 448:579-582. doi:10.1038/nature06017.
28. SSN (2017) Servicio sismológico nacional. Instituto de Geofísica, Universidad Nacional Autónoma de México, México. doi:10.21766/SSNMX/SN/MX.
29. Suárez G, Santoyo MA, Hjorleifsdottir V, Iglesias A, Villafuerte C, Cruz-Atienza VM (2019) Large scale lithospheric detachment of the downgoing Cocos plate: the 8 September 2017 earthquake (M 8.2). Earth Planet Sci Lett 509:9-14. doi:10.1016/j.epsl.2018.12.018.
30. Takemura S, Kubo H, Tonegawa T, Saito T, Shiomi K (2019) Modeling of long-period ground motions in the Nankai subduction zone: model simulation using the accretionary prism derived from oceanfloor local s-wave velocity structures. Pure Appl Geophys 176:627-647. doi:10.1007/s00024-018-2013-8.
31. van der Elst NJ, Brodsky EE (2010) Connecting near-field and far-field earthquake triggering to dynamic strain. J Geophys Res: Solid Earth 115:B07311. doi:10.1029/2009JB006681.
32. Wessel P, Smith WHF (1998) New, improved version of generic mapping tools released. Eos Trans Am Geophys Union 79:579. doi:10.1029/98eo00426.
33. Ye L, Lay T, Bai Y, Cheung KF, Kanamori H (2017) The 2017 Mw 8.2 Chiapas, Mexico, Earthquake: energetic slab detachment. Geophys Res Lett 44:11,824-11,832. doi:10.1002/2017gl076085.
34. Zigone D, Rivet D, Radiguet M, Campillo M, Voisin C, Cotte N, Walpersdorf A, Shapiro NM, Cougoulat G, Roux P, Kostoglodov V, Husker A, Payero JS (2012) Triggering of tremors and slow slip event in Guerrero, Mexico, by the 2010 Mw 8.8 Maule, Chile, earthquake. J Geophys Res: Solid Earth 117:B09304. doi:10.1029/2012jb009160.

Figures

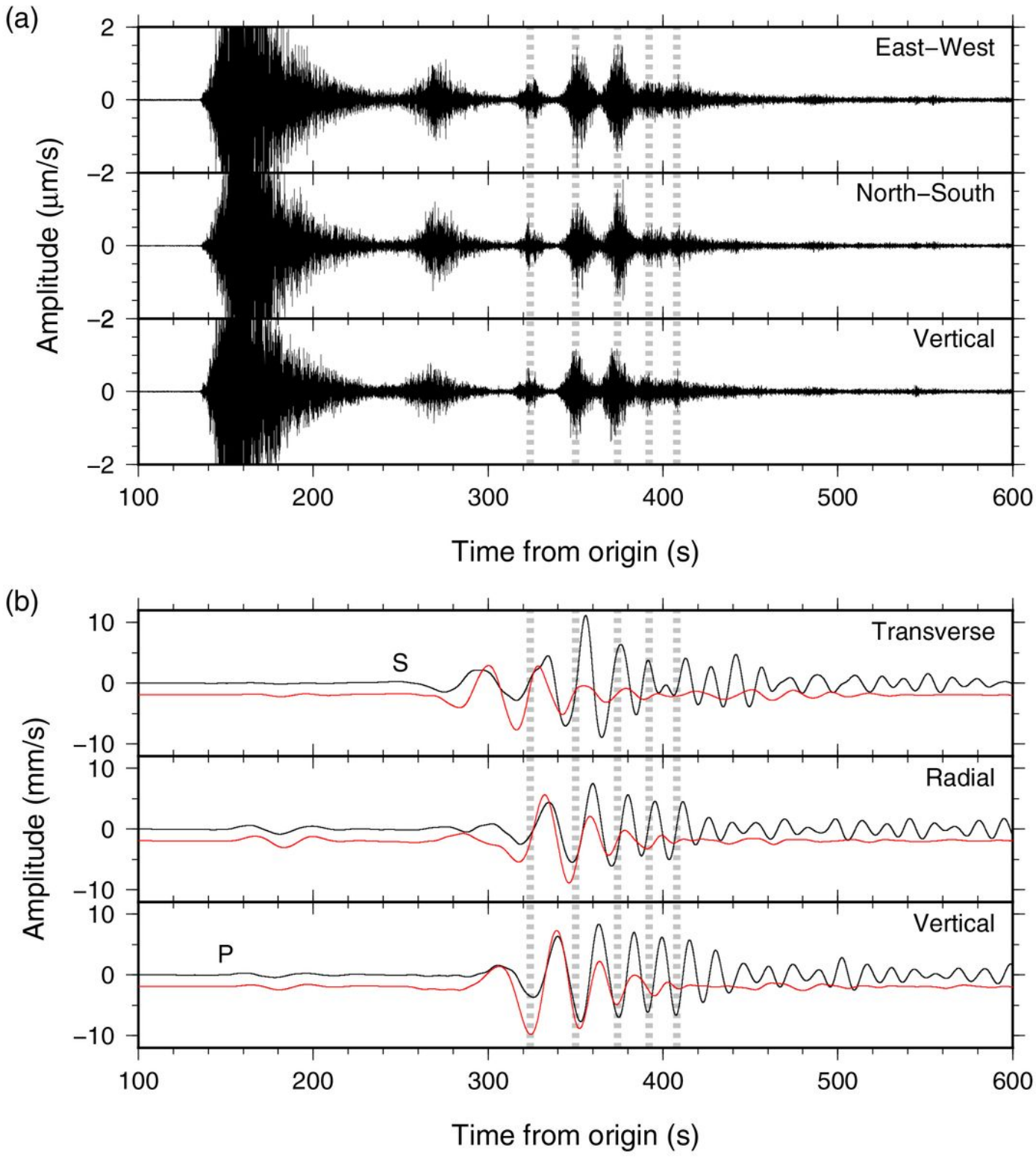

Figure 1

Velocity waveforms for the Mw8.2 Tehuantepec earthquake of September 8, 2017 (UT). (a) Waveforms representing the east-west, north-south, and vertical components, high-pass filtered at 8 Hz, recorded at the National Seismological Service (SSN) of Mexico station CJIG (Figure 2). (b) Waveforms representing the transverse, radial, and vertical components, bandpass filtered between 0.01 and 0.10 Hz. Recorded

waveforms are in black, and simulated waveforms are in red. The vertical dashed lines in gray correspond to the large peaks of triggered tremors.

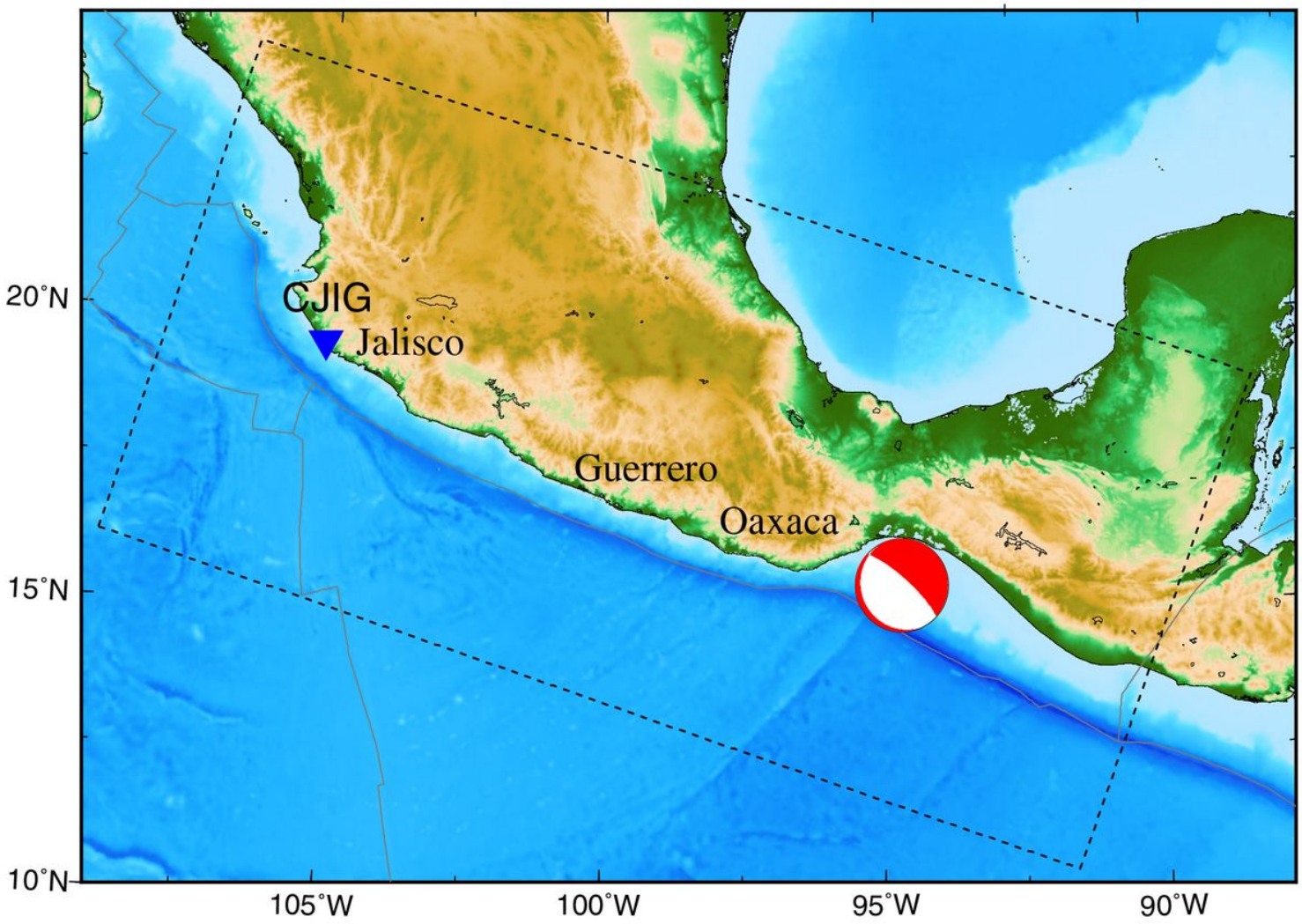

Figure 2

Map showing the study region. The focal mechanism of the 2017 Tehuantepec earthquake from the global CMT catalog is indicated. An inverted triangle shows the position of the SSN station CJIG. Synthetic wavefields of the 2017 Tehuantepec earthquake are calculated in the region bounded by the dashed rectangle. Solid lines show plate boundaries (Bird 2003).

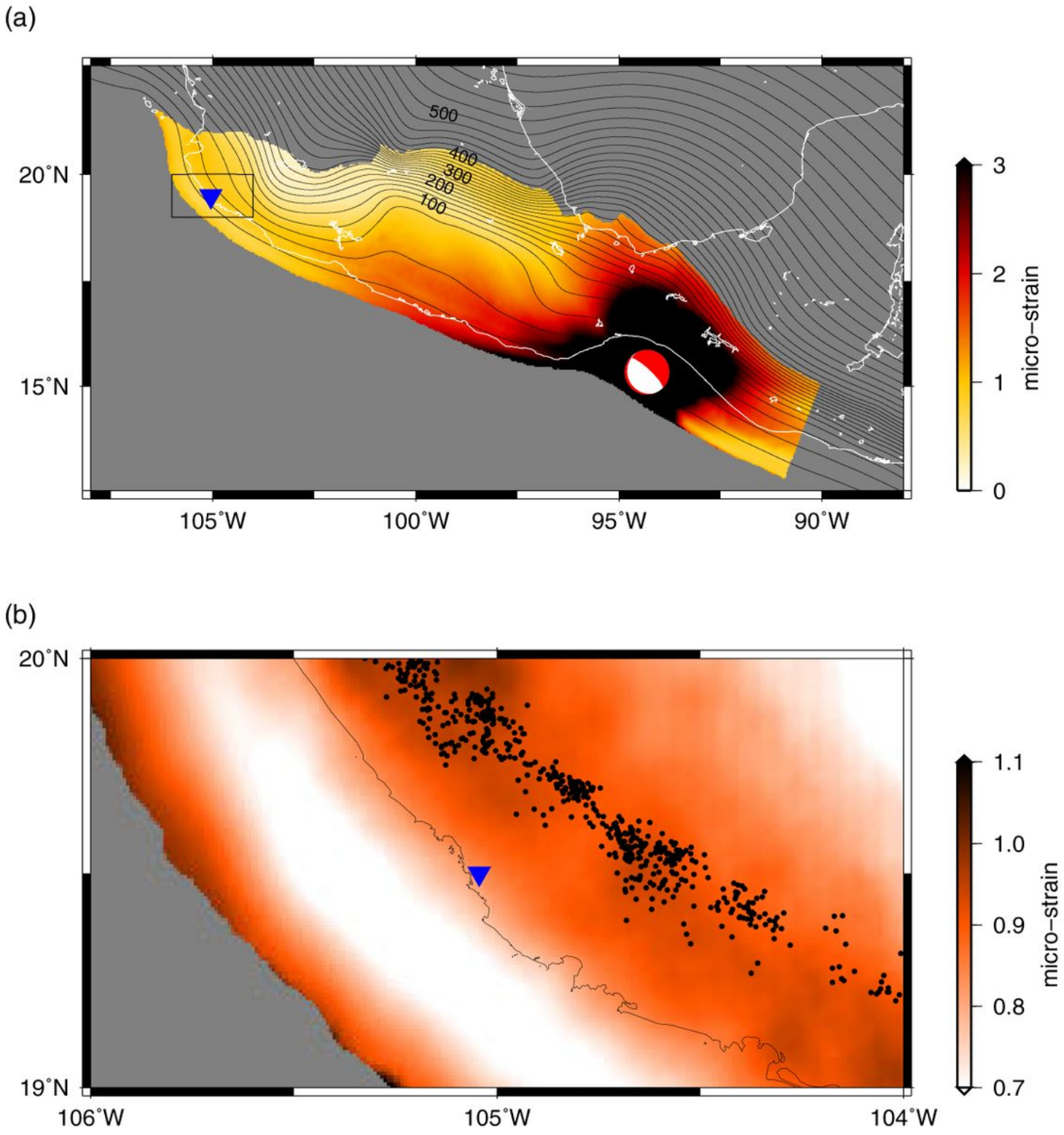

Figure 3

Maximum magnitudes of the strain tensor eigenvalues at depths along the slab top. The contour lines in (a) show the depths of Slab2 and those obtained by extrapolation, in km. In the magnified map in (b), the locations of tectonic tremors by Idehara et al. (2014) are indicated by black dots. Station CJIG is indicated by a blue inverse triangle.

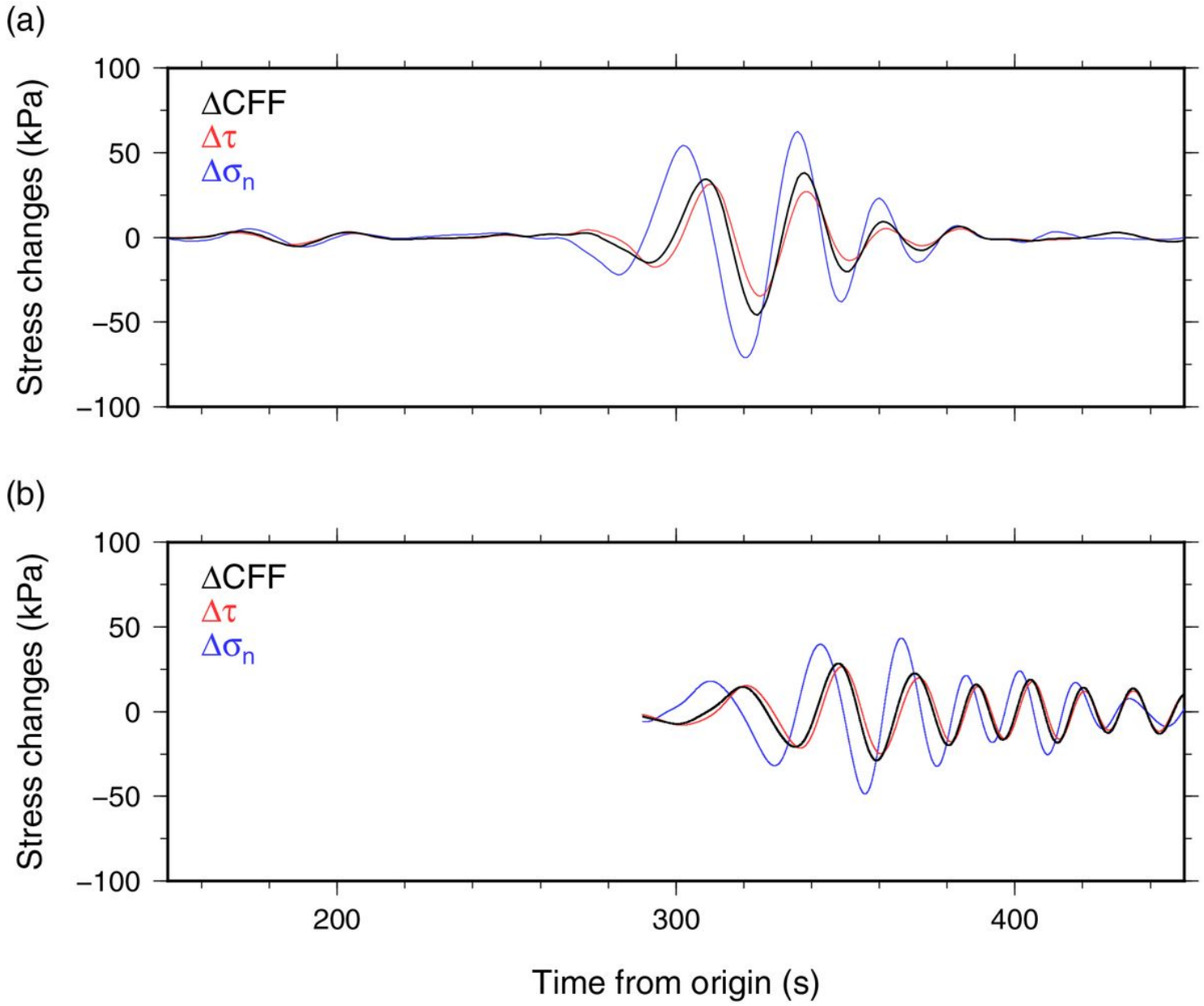

Figure 4

Stress changes resolved for a mechanism of tremor. Δσn represents the normal stress change, Δτ is the shear stress change in the slip direction, and ΔCFF is the Coulomb failure function change for the shear slip on the plate interface at a depth of 45 km. (a) Simulated values at the location estimated by the median epicenter of background tremors. (b) Values estimated from the recorded waveforms beneath station CJIG.

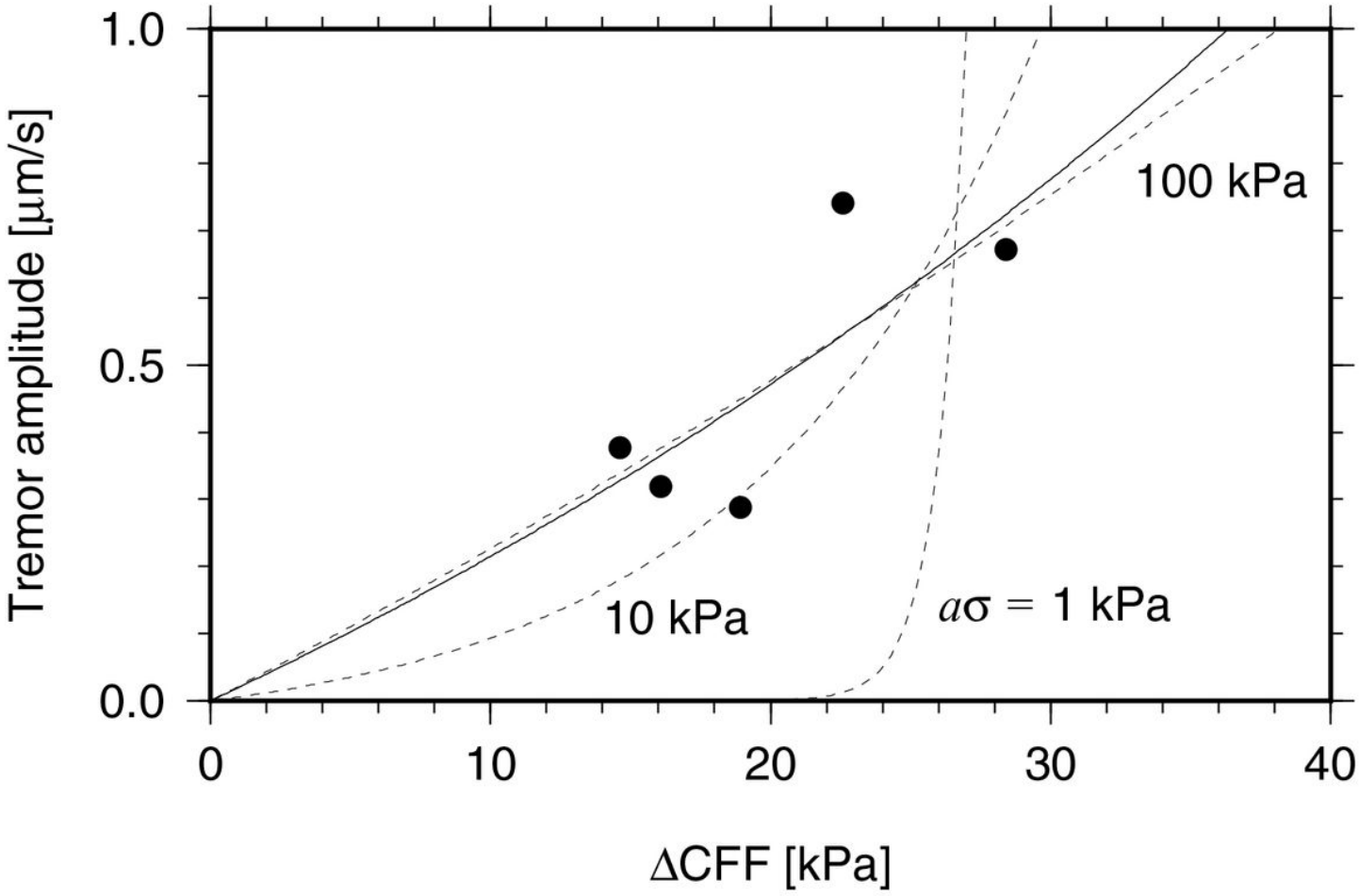

Figure 5

Relationship between the peak velocity amplitude of the triggered tremor and the peak Coulomb failure stress changes. The slid line represents the regression fit with aσ = 56.84 kPa and dotted lines represent the theoretical relationship for aσ = 1, 10, and 100 kPa.

Supplementary Files

This is a list of supplementary files associated with this preprint. Click to download.

- Additionalfiles.docx
- graphicalabstract.jpg
- Simulatedwavefields.mp4